Target-Specificity and Repeatability in Neuro-Cardiac-Guided TMS for Heart-Brain Coupling

Zi-Jian Feng[a, b, c, 1], Sandra Martin[c, 1], Ole Numssen[b, c, *], Konstantin Weise[b, d], Ying Jing[b, c], Gerasimos Gerardos[c], Carla Martin[b, e], Gesa Hartwigsen[c, f, +], Thomas R. Knösche[b, g, +]

[a] TMS center, Deqing Hospital of Hangzhou Normal University, Deqing 313200, Deqing, China.

[b] Methods and Development Group Brain Networks, Max Planck Institute for Human Cognitive and Brain Sciences, Stephanstr. 1a, 04103 Leipzig, Germany.

[c] Research Group Cognition and Plasticity, Max Planck Institute for Human Cognitive and Brain Sciences, Stephanstr. 1a, 04103 Leipzig, Germany.

[d] Institute of Electrical Energy Technology, Leipzig University of Applied Sciences, HTWK, Wächterstraße 13, 04107, Leipzig, Germany.

[e] Institute of Computer Science, Martin-Luther-Universität Halle-Wittenberg, Von-Seckendorff-Platz 1, 06120, Halle, Germany.

[f] Wilhelm Wundt Institute for Psychology, Leipzig University, Neumarkt 9-19, D-04109, Leipzig, Germany.

[g] Technische Universität Ilmenau, Institute of Biomedical Engineering and Informatics, Gustav-Kirchhoff Str. 2, DE-98693, Ilmenau, Germany.

[1, +] These authors contributed equally to this work.

[*] Corresponding author, E-mail address: numssen@cbs.mpg.de (O. Numssen).

Abstract

The dorsolateral prefrontal cortex (DLPFC) is a principal target for repetitive transcranial magnetic stimulation (rTMS) in the treatment of major depressive disorder, with therapeutic effects hypothesized to be mediated by the connectivity between the DLPFC and the subgenual anterior cingulate cortex (sgACC). Interestingly, these depression-related hubs are also part of the heart-brain axis, thus potentially rendering the stratification of individual depression targets possible by tapping into short-term heart rate modulation after DLPFC stimulation. Recently, a set of stimulation protocols has been proposed to objectively quantify these downstream effects. While these neuro-cardiac-guided TMS protocols (NCG-TMS) are promising to improve clinical responses, rigorous, third-party assessments of these approaches including replicability, robustness, and the impact of stimulation side-effects are critically missing. Here, we employed a 10 Hz TMS protocol (NCG-TMS 2.0) across three sessions to evaluate the effects of stimulation intensity and DLPFC target specificity on heart–brain coupling (HBC) in a cohort of healthy participants. Our results demonstrate a significant nonlinear increase in HBC with higher stimulation intensity, with the F3 lateral and F3 posterior targets eliciting more robust effects than the sham condition. For the first time, we are able to demonstrate reliable target- and intensity-specific HBC modulation across multiple NCG-TMS 2.0 sessions. Although the repeatability within subjects was limited when including the initial session, subsequent sessions yielded consistent results for the F3 anterior and F3 lateral targets at higher intensities. Although pain and other side effects influenced HBC, they did not fully account for the observed modulation of HBC. These findings underscore the critical role of spatial specificity and stimulation intensity in modulating heart–brain interactions and offer a potential framework for optimizing individualized rTMS treatment protocols for depression.

1. Introduction

Repetitive transcranial magnetic stimulation (rTMS) is a non-invasive neuromodulation technique widely used to treat neurological and psychiatric disorders, particularly major depressive disorder (Lefaucheur et al., 2020). rTMS induces plasticity, resembling long-term potentiation and long-term depression, thereby affecting both physiological and cognitive functions (Rossini et al., 2015). Although typically applied to target circumscribed cortical areas (Numssen et al., 2023), stimulation effects often propagate beyond the stimulation site through neural network connections, modulating activity in remote brain regions, including subcortical structures (Feng et al., 2022; Martin et al., 2023).

Major depressive disorder is considered a network disorder, involving dysregulated neural circuits rather than isolated brain regions (Spellman & Liston, 2020). A hallmark of this disorder is reduced vagal activity, leading to elevated heart rate (HR) (Berger et al., 2012) and reduced heart rate variability (HRV) (Koenig et al., 2016), reflecting a disrupted heart-brain axis. The prefrontal cortex plays a central role in cardiovascular autonomic regulation, as demonstrated by pharmacological blockades, lesion studies, and neuroimaging findings in humans and animals (Schmausser et al., 2024; Thayer & Lane, 2009; Verberne & Owens, 1998). Meta-analyses consistently underscore the crucial role of the prefrontal cortex in HRV

regulation, highlighting its significance in heart-brain interactions (Thayer et al., 2012).

The frontal–vagal network theory (Iseger, van Bueren, et al., 2020) links cortical regions and autonomic function, suggesting that the dorsolateral prefrontal cortex (DLPFC), subgenual anterior cingulate cortex (sgACC), and the vagus nerve (VN) jointly contribute to the pathophysiology of major depressive disorder and autonomic regulation. In clinical applications, the DLPFC is a key target for rTMS due to its role in emotional and cognitive regulation and its connectivity with the sgACC (Fox et al., 2012). Accordingly, stronger negative DLPFC-sgACC correlations have been associated with better clinical outcomes (Cole et al., 2022; Grosshagauer et al., 2024).

Building on these insights, Neuro-Cardiac-Guided TMS (NCG-TMS) was developed to target the frontal-vagal pathway (Cole et al., 2022; Grosshagauer et al., 2024; Iseger et al., 2017; Iseger et al., 2021; Iseger, van Bueren, et al., 2020). By assessing parasympathetic activity, such as HR changes, NCG-TMS offers a functional outcome measure analogous to motor evoked potentials (MEPs) in primary motor cortex stimulation, reflecting the targeting accuracy of the DLPFC-sgACC network (Cheng et al., 2024; Jiao et al., 2024; Kaur et al., 2020). This approach seeks to optimize therapeutic outcomes by personalizing stimulation parameters based on individual neuro-cardiac coupling levels.

Studies reveal site-specific effects within the (pre-)frontal cortex, with the largest HR decelerations observed at the DLPFC (Zwienenberg et al., 2021). While DLPFC stimulation reduces depressive symptoms, the precise clinical significance of its influence on cardiac autonomic modulation remains unclear. Some studies report a positive correlation between HR decelerations and clinical response (Iseger, Arns, et al., 2020), while others find no significant relationship (Alario et al., 2023, 2024). TMS-induced HR deceleration appears to occur almost immediately, likely due to fast conduction via myelinated vagus nerve fibers, in contrast to slower sympathetic pathways (Iseger, van Bueren, et al., 2020). This suggests that specific TMS parameters could entrain cardiac rhythms as a function of the TMS cycle time (Thut et al., 2011). During rTMS trains, HR may decelerate and recover during inter-train intervals, producing a rhythm that reflects top-down modulation of HR by the brain (E. Dijkstra et al., 2023; Rouwhorst et al., 2022).

This so-called NCG-TMS 2.0 protocol has been proposed as an effective approach to address interindividual differences in patients with major depressive disorder, enabling precise targeting without requiring costly functional magnetic resonance imaging (fMRI) scans or computationally intensive analyses. Variability in Heart-Brain Coupling (HBC) power across stimulation intensities has been observed (E. Dijkstra et al., 2023), suggesting its potential as a biomarker for individualized TMS target selection, particularly in regions associated with prefrontal-sgACC connectivity (Dijkstra et al., 2024).

However, prior research has reported inconsistent HBC variability across stimulation intensities, with targets spanning the frontal lobe and parietal regions rather than being confined to the DLPFC, introducing spatial heterogeneity (Dijkstra et al., 2024).

Although the NCG-TMS 2.0 protocol shows significant potential for improving TMS therapy by refining DLPFC-sgACC pathway targeting, larger openly accessible datasets and repeatability estimates are needed to validate these effects. This preregistered study (https://osf.io/8qpv3/) addresses these gaps by

investigating a larger cohort of healthy participants across three NCG-TMS 2.0 sessions, targeting six distinct left DLPFC sites alongside a sham condition. The primary objectives were to: (1) perform a systematic and preregistered replication the results of Dijkstra et al. (2023) and use advanced statistical methods to confirm that heart rate modulation can indeed be induced by NCG-TMS 2.0, (2) evaluate the repeatability across sessions and the generalizability across participants, (3) systematically evaluate the optimal target for NCG-TMS by investigating a wider range of stimulation sites in DLPFC, and (4) openly share the dataset to enhance transparency and support future research. In addition, we provide a first estimation of the direction of the rTMS-induced heart rate change.

By addressing these objectives, this study provides new insight into rTMS-modulated heart-brain interactions, advancing treatment strategies through improved target selection, individualized stimulation protocols, and open access for the research community.

2. Methods

2.1 Participants

Twenty healthy, right-handed participants were recruited. One participant withdrew due to scheduling conflicts, resulting in a final sample size of 19 participants (9 females, aged 18-39 years, mean age 30.3 ± 5.5 years). All participants were right-handed according to the Edinburgh Handedness Inventory (Oldfield, 1971). Before participation, they underwent a medical screening for TMS. Participant inclusion followed the safety guidelines for TMS studies (Rossi et al., 2021). The experiments complied with the Declaration of Helsinki and was approved by the Ethics Committee of the Medical Faculty at Leipzig University (342/23-ek). All participants provided written informed consent before the study and were financially compensated for their participation. The study was pre-registered (DOI: https://doi.org/10.17605/OSF.IO/E3FNY) to enhance transparency and avoid bias.

2.2 Study Design

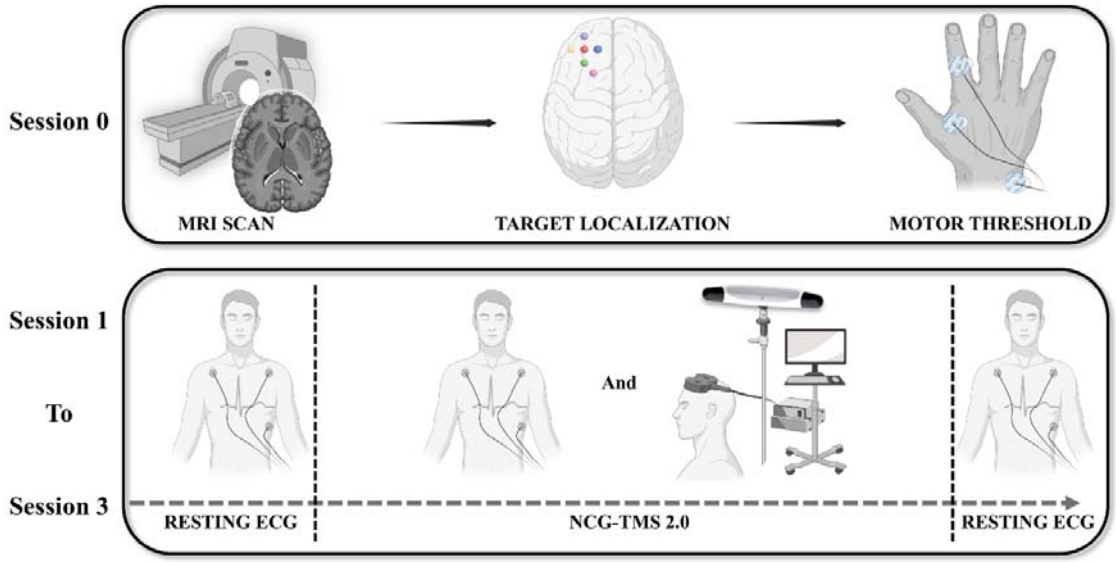

Fig. 1. Overview of the Study Design. Study design comprising a preparatory phase (Session 0) and an experimental phase (Sessions 1 to 3). Session 0 included MRI-based target localization within the DLPFC and determination of motor thresholds for personalized TMS calibration. Sessions 1 to 3 involved electrocardiogram (ECG) recordings before, during, and after stimulation, as well as the application of the NCG-TMS 2.0 protocol at the six identified active targets and one sham stimulation site. Colored circles in the target localization phase indicate the F3 target (in red), F3 lateral (in yellow), F3 medial (in blue), F3 anterior (in purple), F3 posterior (in green), and the 5 cm target (in pink).

The study design comprised two phases: a preparatory phase (Session 0) and the experimental phase (Sessions 1 to 3). In Session 0, participants underwent an MRI scan to acquire high-resolution structural images, which will be used for TMS neuronavigation to guide rTMS in subsequent sessions. Subsequently, individual motor thresholds were determined to calibrate TMS intensity. During sessions 1 to 3, each target included two resting electrocardiogram (ECG) periods surrounding the application of the NCG-TMS 2.0 protocol. The initial resting periods were implemented to establish baseline measures, while the post-stimulation resting periods aimed to mitigate edge effects and ensure the accurate capture of stimulation-induced HBC (Fig. 1).

We applied the 10 Hz dash rTMS protocol from NCG-TMS 2.0, as described by Dijkstra et al. (2023), to the DLPFC targets identified in Session 0. The stimulation protocol consisted of 16 blocks, with 15 active trains per target. Intensity increased in 2% increments of the maximum stimulator output (MSO). Each block included a 10 Hz TMS train lasting 5 seconds, followed by an 11-second inter-trial interval (ITI) (see Fig. 2, Top). The final (15th) intensity was set at 120% of the participant's resting motor threshold (rMT), while the first active intensity was set at 28% MSO below this final level (see Fig. 2, bottom). Prior to the active stimulation, a rest block at 0% MSO was included to establish a baseline.

Our study incorporated specific adjustments to the original NCG-TMS 2.0 protocol by adding rest periods for baseline correction. Specifically, we introduced eight blocks of rest prior to the initiation of the active stimulation. Additionally, two blocks of post-stimulation resting periods were added after the NCG-

TMS 2.0 protocol to mitigate edge effects when calculating HBC power.

To assess the repeatability of HBC over time, each participant completed three experimental sessions, with an interval of 10.8 ± 9.5 days between sessions. We stimulated six cortical regions within the left DLPFC to investigate the spatial specificity of the NCG-TMS 2.0 protocol. The precise definitions of these target locations, labeled Beam F3 (short: F3), F3 anterior, F3 posterior, F3 lateral, F3 medial, and 5-cm rule method (short: 5cm), will be given in Section 2.4 (see Fig. 1 for the target locations). Two of them (F3 and 5cm) have been investigated previously by Dijkstra et al. (2023).

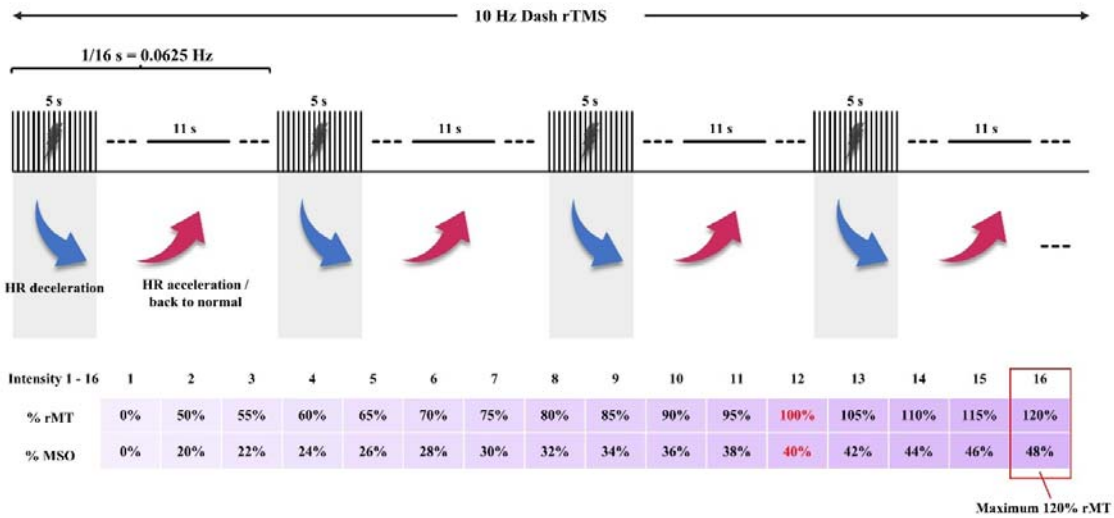

Intensity 1 - 16	1	2	3	4	5	6	7	8	9	10	11	12	13	14	15	16
% rMT	0%	50%	55%	60%	65%	70%	75%	80%	85%	90%	95%	100%	105%	110%	115%	120%
% MSO	0%	20%	22%	24%	26%	28%	30%	32%	34%	36%	38%	40%	42%	44%	46%	48%

Fig. 2. 10 Hz Dash rTMS Protocol from NCG-TMS 2.0. Top: The 10 Hz dash protocol consists of 16 second cycles, each comprising a 5-second-train of 10 Hz rTMS followed by an 11-second pause. This results in an entrainment frequency of 1/16 s = 0.0625 Hz. Bottom: A full sweep includes 16 seconds of rest (0% MSO intensity) and 15 active stimulation intensities, shown for an exemplary participant with an rMT of 40% of the maximum stimulator output (MSO). The protocol administers 15 increasing intensities in steps of 2% MSO. The final intensity level is set to 120% rMT, which equates to 48% MSO for this individual. HR, heart rate; rMT, resting motor threshold.

2.3 Power Analysis

Our within-subject factorial design includes three factors: Target, Intensity, and Session. This resulted in 7 (Target) * 16 (Intensity) * 3 (Session) = 336 measurements per participant. Based on an anticipated small effect size of 0.1, with alpha set to 0.05 and statistical power to 0.8, the minimum required sample size was calculated to be 16 participants (https://aaroncaldwell.us/SuperpowerBook/). To account for an estimated 20% dropout rate due to technical difficulties or participant discomfort (e.g., pain), we invited 20 participants to complete all three sessions.

2.4 Data Acquisition and Experimental Setup

For each participant, MRI scans were acquired using a 3T MRI scanner (Siemens Verio or Skyra fit) equipped with a 32-channel head coil to obtain high-resolution T1-weighted images. The scanning parameters were as follows: T1: MPRAGE ADNI with 176 sagittal slices; repetition time (TR): 2.3 s; echo

time (TE): 2.98 ms; field of view (FoV): 256 mm; voxel size: 1 x 1 x 1 mm; no slice gap; flip angle: 9°. If high-quality scans (less than two years old) were available in the in-house database, they were used instead of new acquisitions.

For TMS, we used a MagPro X100 stimulator (MagVenture, Farum, Denmark) with a passively cooled MCF-B65 figure-of-eight coil. Sham stimulation was applied using the corresponding sham coil (MCF-P-B65), which generates the same acoustic noise as the active coil but reduces the magnetic field strength by approximately 80%. Participants were blinded to the type of stimulation (active vs. sham). Coil positioning was guided by a neuro-navigation system (TMS Navigator, Localite, Sankt Augustin, Germany) with a Polaris Spectra camera (NDI, Waterloo, Canada), and coil placements were recorded for each TMS pulse.

Prior to testing, participants were seated and instructed to remain relaxed, minimize movement, and refrain from speaking. Electrocardiogram (ECG) electrodes were placed as follows: the ground electrode above the left breast, the reference electrode above the right breast, and the active electrode below the left breast. ECG data were recorded during stimulation using the REFA8 68-channel amplifier system (TMSi, Oldenzaal, The Netherlands) with Brain Vision Recorder software (Brain Vision, MedCaT B.V.). A visual inspection of the ECG trace was conducted to ensure signal quality before the experiment began. After each rTMS session, participants completed a questionnaire assessing potential side effects (Giustiniani et al., 2022). Total scores of the side effects are presented in the supplementary materials (Fig. S1).

At the beginning of the first session, the resting motor threshold (rMT) for the first dorsal interosseous (FDI) muscle was manually determined as the minimum stimulator intensity required to elicit motor evoked potentials (MEPs) with an amplitude of at least 50 μV in 5 out of 10 consecutive TMS pulses, following the relative frequency method (Rossini et al., 2015). Electromyography (EMG) signals from the right FDI muscle were used to detect MEPs during the rMT determination procedure.

The individual F3 target was identified using the Beam F3 algorithm and software (Eva Dijkstra et al., 2023; E. Dijkstra et al., 2023; Mir-Moghtadaei et al., 2015). Four additional targets were defined surrounding the F3 location, positioned 2 cm in the anterior, posterior, lateral, or medial directions. The 5cm target was defined as the stimulation site where the TMS coil was positioned 5 cm anterior to the optimal scalp location for eliciting activation of the FDI muscle (Eva Dijkstra et al., 2023; E. Dijkstra et al., 2023; Pascual-Leone et al., 1996). If the 5cm target was within 1 cm of any other target, it was excluded. The coil orientation for all targets was set at an angle of 45° relative to the parasagittal plane, with the coil handle pointing posteriorly.

To assess participants' tolerance, a single 10 Hz TMS train at 120% rMT—the maximum stimulation intensity of the protocol—was applied to each target before rTMS administration. Unpleasantness levels were assessed using the Discrete Visual Pain Rating Scale (DVPRS) (Polomano et al., 2016). Pain scores for each target are shown in Figure S2. If pain scores exceeded 6 (out of 10) points (indicating a level above 'moderate'), the coil angle was adjusted from 45° to 90° to reduce discomfort. This adjustment was necessary for six participants. Despite these modifications, five targets from three participants were ultimately excluded due to persistent pain scores exceeding 6 points. Sham stimulation was performed at

one of the five targets—F3 or one of the four surrounding targets—randomly assigned for each participant. Sessions 2 and 3 consisted of repetitions of both active and sham NCG-TMS 2.0 protocols conducted during Session 1. The target order was randomized across participants, and the same order was maintained across all sessions.

2.5 Data Analysis

2.5.1 Individual Heart-Brain Coupling

The ECG data analysis in this study was adapted from the original analyses (https://github.com/brainclinics/HBC) by Dijkstra et al. (2023): Initially, ECG signals were processed using a bidirectional fourth-order Butterworth bandpass filter with a frequency range of 0.5 to 20 Hz, effectively removing low-frequency noise and high-frequency artifacts. The R peak, a prominent upward deflection in the QRS complex of the ECG signal that represents ventricular depolarization, was identified using the 'signal.findpeaks' function from SciPy (Virtanen et al., 2020) along with the ‘ecg_peaks’ function from NeuroKit2 toolbox (Makowski et al., 2021). Manual correction was subsequently applied to improve detection accuracy. Signals requiring manual corrections for more than 10% of the total R peaks for any target were excluded from the analysis, and one target from a participant was excluded due to insufficient usable signal.

Following R peak detection, the time differences between two consecutive R-waves in the ECG (RR intervals) were corrected for ectopic beats, and the HR was computed for each RR interval. To smooth the HR data, a moving average of five consecutive HR values was applied, followed by interpolation across all ECG time points. A 1.5-second Hann window was applied to reduce abrupt fluctuations and enhance overall data consistency.

Time-frequency analysis was conducted using the 'tfr_array_morlet' function from MNE-Python (Gramfort et al., 2013). This generated a time-frequency representation of the ECG signal across a frequency range of 0.02 to 0.18 Hz, with increments of 0.0025 Hz. High temporal resolution (3 cycles) and high frequency resolution (10 cycles) allowed for a detailed examination of low-frequency oscillations. Data padding was applied at both the start and end of the sequence to facilitate the analysis of these low-frequency components.

HBC was quantified by the power at 0.0625 Hz corresponding to one TMS cycle comprising 5 seconds of stimulation and 11 seconds of rest. The analysis was applied to all 26 blocks of ECG data. However, only the 16 blocks corresponding to the NCG-TMS 2.0 protocol were retained, while the initial 8 resting blocks and the last 2 resting blocks were excluded to mitigate edge effects. All analyses were conducted using the raw values of HBC power. The high frequency resolution HBC value for each block was then calculated and used for subsequent analyses. Plots for each target across all three sessions for each participant are provided in the supplementary materials (Fig. S3).

2.5.2 Mixed-Effects Regression Analysis

To analyze the relationship between HBC power of each block and our experimental factors (stimulation intensity and target location) as well as nuisance variables (pain and other side effects), we used mixed-

effects regression. Plotting the raw data per target and session suggested a non-linear relationship between stimulation intensity and HBC power (Fig. S4). To account for this nonlinearity, we set up a generalized additive model (GAM). GAMs determine the optimal shape of the curve fit (i.e., the degree of *smoothness*) for non-linear responses via penalized regression. This data-driven adjustment became necessary as the observed non-linearity (Fig. S4) violated the assumptions of the pre-registered ANOVA approach, making GAMs a more appropriate choice for modeling these effects. The GAM was fitted with a Gamma distribution and a log link function to account for the non-normal distribution of HBC power. This transformation was determined as appropriate based on distribution diagnostics using the package fitdistrplus (Delignette-Muller & Dutang, 2015) to ensure residual normality and homoscedasticity. We included both fixed and random effects in the GAM to appropriately model the data structure and dependencies. The model contained main effects for *session*, *target*, and percentage intensity of MT (*%MT*) as well as the interaction of *target* and *%MT*. We further included two covariates: (i) per participant and target assessed *pain scores* to account for a potential interdependence of HBC with higher pain sensations, and (ii) a sum score of the per participant, session, and target measured *side effects*, which summarize sensations such as headache, nausea, and skin sensation. Moreover, we included the interaction of *%MT* and *pain*, aiming to identify a potential modulation of HBC through intensity-dependent pain values.

The splines of the continuous predictors *%MT*, *pain*, and *side effects* were fitted with thin-plate regression splines. The interaction of *%MT* and *target* was fitted with by-target individual splines, resulting in individual curves for each level of *target*. For the interaction of *%MT* and *pain* a tensor product interaction term with a cubic regression spline was used to accommodate the differing scales of both variables. The number of basis dimensions for each smoothing spline was checked via model diagnostics available in *mgcv* after the first model set-up and appropriately updated to reach $p > 0.05$ to avoid overfitting. Random effects included random intercepts for *participant* and *block*, and by-participant random slopes for *session* (eq. 1).

$$
\begin{aligned}
\textit{HBC Power} \sim \quad & \textit{Session} + \\
& \textit{Stimulation Target} + \\
& \textit{\%MT} + \\
& \textit{Pain Score} + \\
& \textit{Side Effects} + \\
& \textit{Stimulation Target} : \textit{\%MT} \\
& \textit{Pain} : \textit{\%MT} + \\
& (1 + \textit{Session} \mid \textit{Participant}) + \\
& (1 \mid \textit{Block})
\end{aligned}
\qquad \text{(eq. 1)}
$$

We also fitted a standard linear regression model to confirm our results without relaxing the linearity assumption. To this end, a generalized linear mixed-effects model (GLMM) with a Gamma distribution and a log link function was set up with the same fixed and random effects as the GAM (see eq. 1).

In all regression analyses, we employed simple contrast coding for categorical factors and mean-centering for continuous predictors to ensure interpretability and comparability of the results. Additionally, we applied a false discovery rate (FDR) correction to the p-values obtained from the model summaries to

control for multiple comparisons. Analyses were carried out in R version 4.4.0 (R Core Team, 2023) using the packages lme4, mgcv, modelbased, ggeffects, performance, and sjPlot (Bates et al., 2015; Lüdecke, 2018, 2024; Lüdecke et al., 2021; Makowski et al., 2020; Wood, 2017).

2.5.3 Repeatability Analysis

To assess the repeatability of block-level measurements across multiple sessions for each target, we calculated the Intraclass Correlation Coefficient (ICC) using a two-way random-effects model. This model assumes that both targets and sessions were selected at random, which allows for generalization beyond the specific samples studied. Specifically, we assessed the consistency of HBC power values across three sessions for each block within a target. The ICC formula used is as follows:

$$ICC = \frac{MSb - MSw}{MSb + (k-1)MSw} \qquad (\text{eq.}\,2)$$

MSb (Mean Square Between Subjects) quantifies the variability in measurements between participants, averaged across all sessions, MSw (Mean Square Within Subjects) reflects the variability within individual participants across sessions, and k represents the number of sessions (here, $k = 3$).

The ICC was computed using the Pingouin Python package (Vallat, 2018), which employs an ANOVA-based approach to estimate the variance components. This analysis was performed to determine the repeatability of block-level measurements across repeated sessions, thereby providing insight into the stability and consistency of TMS-induced HBC responses.

High ICC values indicate that most of the observed variability is driven by between-participant differences, suggesting good repeatability. Conversely, lower ICC values imply substantial variability within participants across sessions, potentially undermining the repeatability of these measurements. In addition, we calculated pairwise ICC values between each session to further explore the consistency between individual sessions.

2.5.4 Analyses of Heart Rate Modulation Direction

Previous studies have demonstrated that vagus nerve stimulation elicits a rapid autonomic response within the same cardiac cycle, with effects typically lasting only 1–2 heartbeats (Iseger, van Bueren, et al., 2020). Similarly, pupil size, a well-established indicator of autonomic nervous system activity, has been shown to respond to TMS within a 2-second window (Niehaus et al., 2001).

Drawing on these findings, the HR analysis was conducted using a 2-second post-stimulation window to capture potential rapid autonomic responses. For pre-train HR, two reference intervals were employed: (1) Baseline, which excluded data from the first two blocks of each session to ensure HR stability; (2) Pre-train, defined as the 2-second window immediately preceding stimulation. If two consecutive R peaks could not be identified within the defined 2-second window for HR calculation, HR was instead determined using the first two consecutive R peaks identified either before or after the stimulation period.

3. Results

We report data from 19 subjects, who participated in three sessions with 7 individual stimulation targets. Due to overlap with other targets (see section 2.4), the 5 cm target was recorded as an individual target only in 9 subjects. Plotting the raw data with an overlaid smooth function revealed a mostly non-linear relationship between target, stimulation intensity, and HBC (Fig. S4) with some variance regarding the magnitude of HBC between subjects (Fig. S3).

3.1 GAM and GLMM Analysis

We applied both a GAM and a GLMM to explore, (1) whether there is a significant intensity- and target-dependent modulation of the heart rate by TMS (heart-brain coupling, HBC), (2) to what extent this effect can be explained by pain or other side effects, which are also potentially intensity-dependent, and (3) whether any intensity effect on HBC is specific to particular target positions in the DLPFC. To this end, we tested how well HBC is explained by the experimental variables *stimulation target*, *session*, and *intensity (%MT)*, as well as the nuisance variables *pain* and *side effects*. Comparing the linear and non-linear models, the GAM demonstrated a superior fit as indicated by a lower Akaike Information Criterion (AIC) value, even with more degrees of freedom (AIC_{GAM} = 116,683.0, df_{GAM} = 108.42, AIC_{GLMM} = 117,027.9, df_{GLMM} = 27.0). Therefore, we present the GAM results below. The GLMM results corroborated the GAM (see Table S1 for details).

Effects of Session and Target: The GAM included parametric terms for session and stimulation target. Results revealed little differences in HBC of session 2 and 3 relative to session 1 ($\beta_{session\ 2} = 1.13$, $p = 0.810$, $\beta_{session\ 3} = 1.02$, $p = 0.981$). Stimulation targets at F3 anterior, lateral, and posterior were associated with increased HBC relative to sham stimulation, while all other targets were linked with decreasing HBC compared to sham (Table 1). After FDR correction, this main effect remained significant for the lateral and posterior F3 targets ($\beta_{F3lat} = 1.46$, $p < 0.001$, $\beta_{F3pos} = 1.18$, $p = 0.033$). In sum, we show that in some targets, HBC is significantly higher compared to sham stimulation.

Effects of Stimulation Intensity, Pain, and Side Effects: The GAM further included smoothing splines for %MT, Pain, and a sum score of Side Effects. Results showed a significant effect on HBC only for side effects ($F_{Side\ Effects} = 13.52$, $p < 0.001$, Table 1). Exploring the smoothing curve of Side Effects revealed an inverted U shape, where for low to moderate values (side effects score ≤ 7.33), HBC increased with the strength of estimated side effects, and for moderate to high values (side effects score ≥ 7.33), HBC decreased (Fig. S5). In sum, we could not prove main effects for %MT and Pain, but for Side Effects, which showed a non-linear relationship with HBC.

Interaction of Stimulation Intensity and Target: Modeling the interaction between %MT and stimulation target showed significant non-linear effects for F3 and surrounding targets ($F3_{ant}$, $F3_{pos}$, $F3_{med}$, $F3_{lat}$; all $p < 0.05$, FDR-corrected, see Table 1), but not for sham stimulation and the 5cm target (Fig. 3a). To assess the magnitude of target-specific effects compared to sham stimulation, we calculated the average difference in HBC power for each target and level of %MT relative to sham, while aggregating over all

other model terms. The results indicated that, averaged across all stimulation intensities, F3 and surrounding targets were associated with a stronger increase in HBC power compared to sham (all $p < 0.05$, FDR-corrected, Fig. 3b). The strongest effect on HBC relative to sham was observed in the posterior, medial, and lateral F3 targets. For example, the posterior F3 target increased HBC by 140 points or 11,145% compared to sham stimulation across all stimulation intensities (estimated marginal mean for F3 posterior: 138.98 points, for sham: -1.26 points in HBC power). In summary, increasing HBC was modulated by the interaction of %MT and targets, showing that F3 and surrounding targets yield higher HBC in a stimulation-dependent manner.

Interaction of %MT and Pain: Results from the GAM revealed a significant non-linear interaction of %MT and pain ($F = 3.48$, $p < 0.001$). To explore this interaction of both continuous predictors, we ran a simple slopes analysis and calculated Johnson-Neyman intervals. Results showed that pain significantly influenced the effect of %MT for low pain values (pain score between 0.67 and 1.33 points; range 0-6) and high pain values (pain scores above 4). For these values, the slope of %MT was positive, thus increasing HBC when pain scores were high (Fig. S6).

To further evaluate the contribution of pain to changes in HBC, we set up two additional models: a GAM without the effect of *%MT*, only including *pain* and its interaction with *stimulation target*, and a GAM without *pain scores* but including *%MT* and its interaction with *target*. Comparing AIC and R^2 values for these models with our final regression model (see eq. 1) showed that the GAM including both terms (*%MT* and *pain*) outperformed the individual models in terms of AIC ($AIC_{MT} = 116{,}729.6$, $df_{MT} = 100.05$, $AIC_{Pain} = 116{,}767.9$, $df_{Pain} = 106.11$, $AIC_{Final\ model} = 116{,}683.0$, $df_{Final\ model} = 108.42$) and R^2 values ($R^2_{MT} = 0.477$, $R^2_{Pain} = 0.465$, $R^2_{Final\ model} = 0.494$). Moreover, the model with %MT provided a better fit than the model including only pain scores (Table S2). In summary, while pain influences the HBC, it does not fully account for the %MT dependence. Moreover, %MT seems to be a stronger predictor than pain alone.

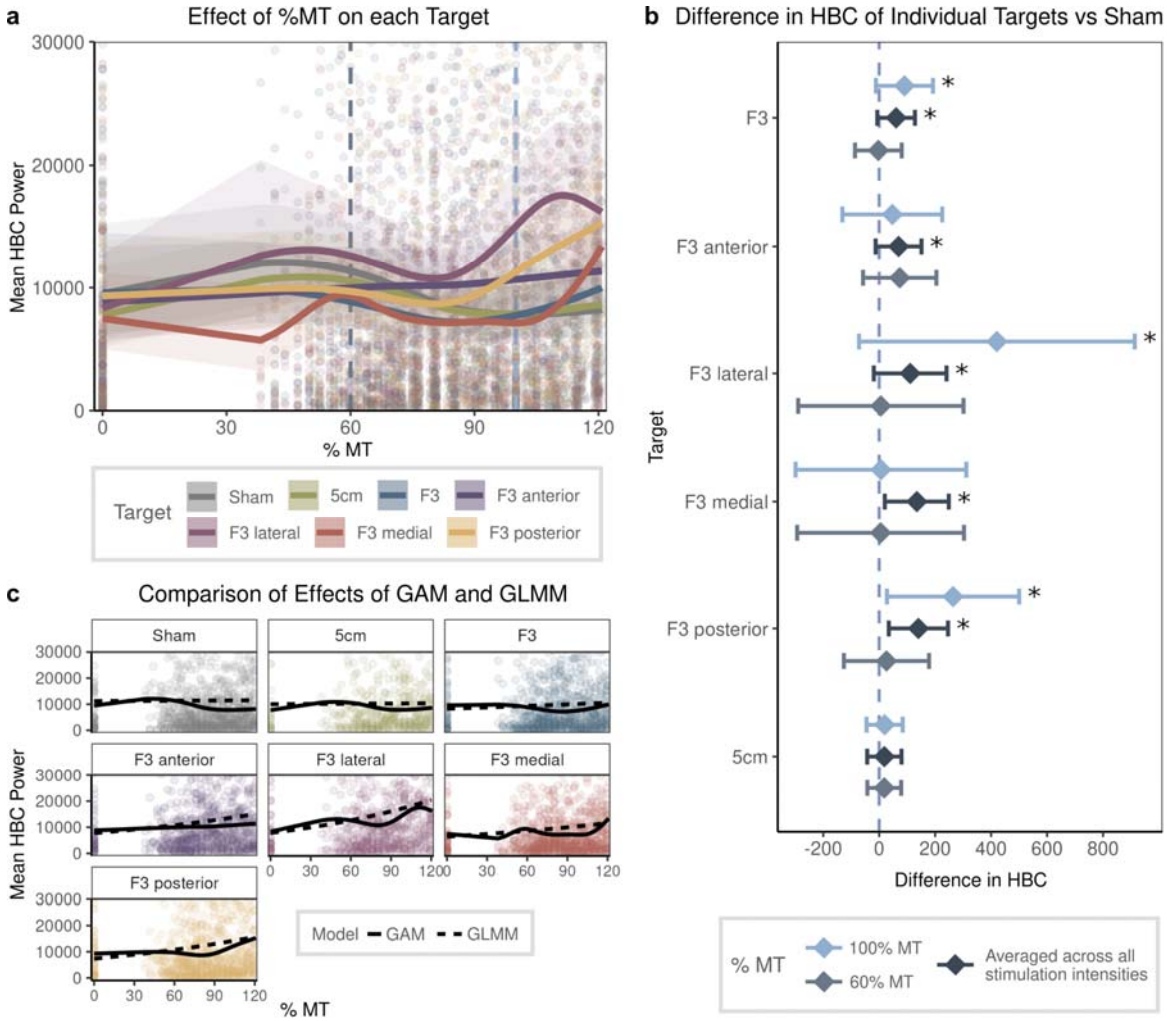

Fig. 3. TMS-induced Heart-brain-coupling across Different DLPFC Stimulation Sites. Panel a displays estimated marginal predictions from a generalized additive model (GAM) for the interaction between stimulation intensity (% rMT) and stimulation target with raw data plotted in the background. Dashed lines show stimulation intensities, for which differences relative to sham were computed (next panel). Panel b illustrates the difference in marginal predictions for different values of % MT per target relative to sham. Significant effects for stimulation intensity at 60% MT and averaged across all stimulation intensities are marked with an asterisk. Stimulation over all F3 targets significantly increased HBC power compared to sham. Panel c compares marginal predictions for each target derived from the GAM and the GLMM. Although both models lead to similar conclusions, the GAM outperformed the GLMM in measures of goodness of fit.

	HBC Power			
Predictors	***Estimate / edf***	***std. Error***	***Statistic***	***p***
Session [Session 2]	1.13	0.31	0.43	8.10e-01
Session [Session 3]	1.02	0.28	0.08	9.81e-01
Target [5cm]	0.97	0.07	-0.39	8.10e-01
Target [F3]	0.92	0.06	-1.13	3.79e-01
Target [F3 anterior]	1.16	0.09	1.99	8.52e-02
Target [F3 lateral]	1.46	0.11	4.88	**5.87e-06**
Target [F3 medial]	0.91	0.06	-1.48	2.26e-01
Target [F3 posterior]	1.18	0.08	2.43	**3.32e-02**
%MT	1.00		2.13	2.26e-01
Pain	1.18		0.05	9.55e-01
Side Effects	8.85		13.52	**0.00e+00**
%MT x Target [Sham]	1.00		0.66	5.74e-01
%MT x Target [5cm]	2.94		0.03	9.96e-01
%MT x Target [F3]	2.43		4.72	**7.78e-03**
%MT x Target [F3 ant]	3.16		2.82	**4.59e-02**
%MT x Target [F3 lat]	4.74		4.17	**1.75e-03**
%MT x Target [F3 med]	6.32		3.05	**7.24e-03**
%MT x Target [F3 pos]	3.67		7.57	**1.16e-05**
%MT x Pain	12.98		3.48	**8.94e-06**
Marginal /Conditional R^2	0.494			

Table 1. Results from the Generalized Additive Model (GAM). Significant effects are marked in bold. For smooths and smooth-by-factor interactions, the table shows effective degrees of freedom (edf) instead of parameter estimates and standard errors. Reported p-values are FDR-corrected.

3.2 Heart-brain Coupling Repeatability of Block-level Measurements across Sessions

ICC was calculated to assess the repeatability of block-level measurements across three sessions for each stimulation target (Fig. 4). Overall, the ICC values exhibited considerable variability across all targets, with the majority of values falling below 0.4 (*moderate repeatability)*, indicating poor repeatability for

block-level measurements across sessions. Despite this general trend of low repeatability, certain targets showed substantial repeatability, especially at higher stimulation intensities.

For the F3 lateral target, a trend of increasing ICC values was observed with higher stimulation intensities, approaching and slightly exceeding the 0.4 threshold, suggesting moderate repeatability at higher intensity levels. For F3 anterior, was above the moderate repeatability even for the entire intensity range. Except for F3 lateral, all other targets, including Sham, showed ICC values consistently below 0.4 at all intensity levels, indicating low repeatability.

To further explore pairwise ICC repeatability, we focused on the F3 anterior and F3 lateral targets, which demonstrated relatively better repeatability. Specifically, the comparison between Session 2 and Session 3 showed ICC values exceeding 0.8 in the later blocks, indicating excellent repeatability at higher stimulation intensities. In contrast, comparisons involving Session 1 consistently yielded ICC values below 0.4, suggesting poor repeatability between Session 1 and subsequent sessions (Fig. 4, right panels). Hence, while repeatability between the first and second sessions was generally low, it was substantially better between subsequent sessions for some targets.

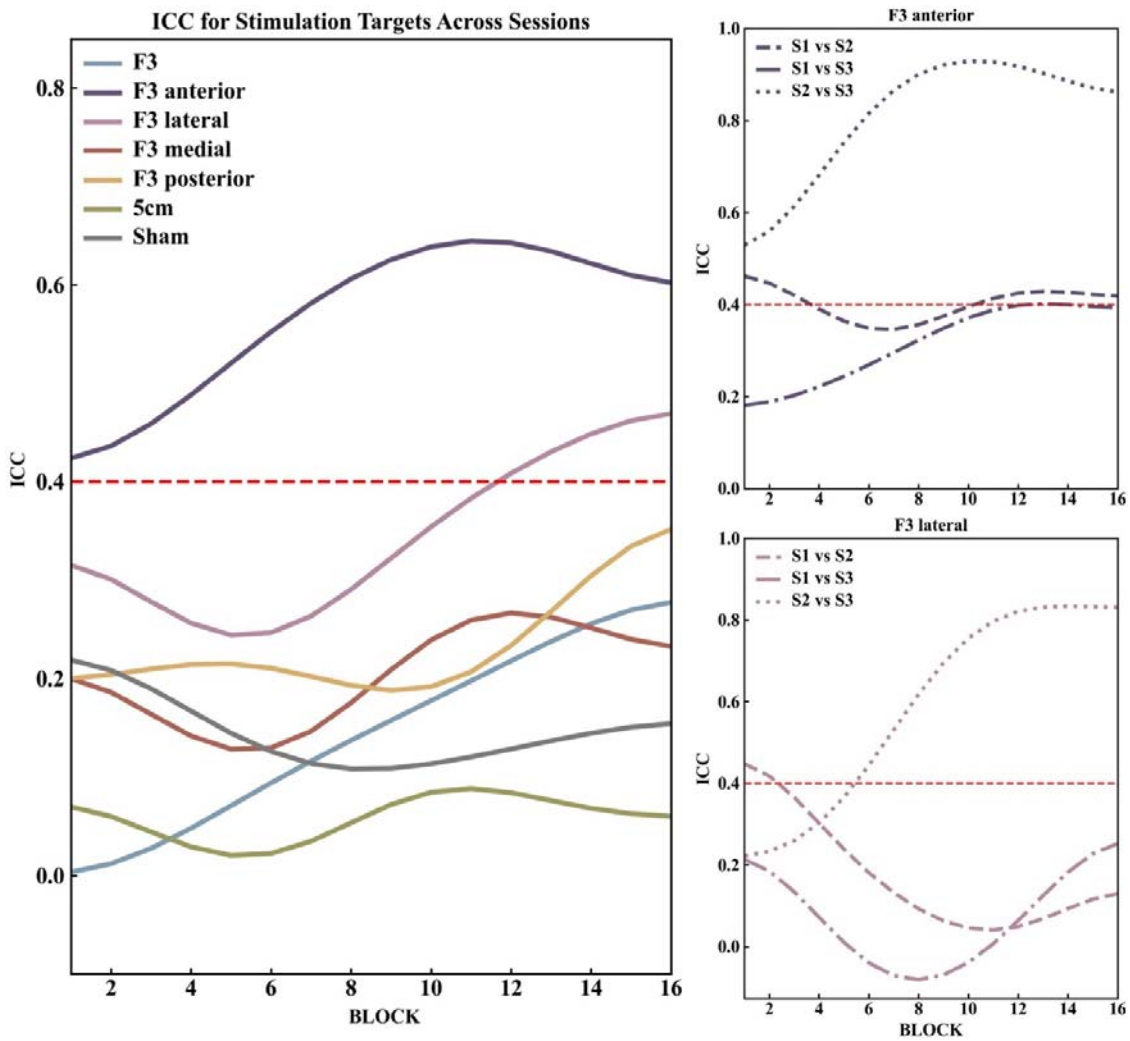

Fig. 4. Intraclass Correlation Coefficients (ICC) for Block-level Measurements. Left: ICC values for different stimulation targets across three sessions. Different colors indicate different stimulation targets. Right: Pairwise ICC values for different session comparisons (solid line: session1 vs session2, dashed line: session1 vs session3, dotted line: session2 vs session3) for F3 anterior (top) and F3 lateral (bottom) stimulation targets. The x-axis represents block numbers, corresponding to increasing TMS stimulation intensities. The red dashed line marks the threshold for moderate repeatability at ICC = 0.4.

3.3 Heart Rate Modulation Direction

As shown in Figure S7, HR changes were analyzed post-train compared to baseline across stimulation targets. Across all targets, HR fluctuations remained minimal, with changes typically within ±2 bpm of the baseline. Notably, high-intensity F3 lateral stimulation was the only condition that consistently and reliably reduced HR. Similar trends were observed in the results for post-train HR changes compared to baseline across sessions and compared to pre-train, as presented in Figures S7–S10.

4. Discussion

NCG-TMS 2.0 is a rhythmic stimulation approach designed to modulate coupling between cardiac and brain activities. This systematic, pre-registered replication employed advanced statistical methods to assess whether heart rate modulation can be reliably induced by the NCG-TMS 2.0 protocol across a larger sample of participants. Our optimized design included baseline periods of rest and a wide range of stimulation targets in the left DLPFC to systematically evaluate the optimal target for NCG-TMS.

Our main findings were as follows: I) For specific targets in DLPFC (F3 and surrounding sites, in contrast to Sham), we found a significant non-linear increase of HBC with stimulation intensity. For some targets (F3 lateral and F3 posterior), there was even a general increase of HBC as compared to Sham. II) There was no systematic session effect on HBC. The within-subject repeatability across sessions was high for F3 anterior and F3 lateral for high stimulation intensities. III) Pain did non-linearly interact with the intensity effect on HBC, while other side effects generally increased HBC irrespective of other factors. However, the effect of TMS intensity was not redundant with pain or other side effects, indicating a causal effect of the cortical stimulation on heart rate.

4.1 Intensity-Dependent and Target-Specific HBC

Our results reveal that heart-brain coupling shows a strong site specificity to stimulation targets around F3 (specifically F3 lateral and posterior see Fig. 3a and 3b) and depends on TMS intensity in a non-linear fashion. This corroborates the findings of Dijkstra and colleagues (2023), who observed a (linear) main effect of intensity. However, the previous study could not show any systematic influence of stimulation target, which may be explained by the absence of a sham condition in the previous study.

However, while HBC power was enhanced for a selection of targets, this metric does not quantify the directionality of the induced heart rate change, i.e., whether heart rate increased or decreased. Further

exploration comparing post-train heart rate to baseline and pre-train suggests that especially high-intensity F3 lateral stimulation reliably reduced the heart rate (Fig. S7-S10), supporting the NCG-TMS 2.0 hypothesis framework (Eva Dijkstra et al., 2023; E. Dijkstra et al., 2023; Dijkstra et al., 2024). This variability in HBC response across targets is consistent with prior studies indicating that individual anatomical differences can significantly influence TMS-induced electric fields and their resulting physiological effects (Numssen et al., 2024).

Notably, a recent study using sgACC-guided frontal targets demonstrated significant HBC modulation, with target locations distributed around F3, though generalizability was limited by spatial heterogeneity and small sample sizes (Dijkstra et al., 2024). Previous NCG-TMS research also demonstrated target specificity in reducing heart rate, demonstrating that stimulation at F3/F4 and FC3/FC4 led to HR reduction, while stimulation at C3/C4 was associated with increased HR (Iseger et al., 2020 for a meta-analysis). In contrast, more recent findings suggest that stimulation at C3/C4 can also reduce HR, with no significant differences between C3/C4 and F3/FC3 when targeting the left hemisphere (Jiao et al., 2024). This implies that the motor cortex may not be an ideal control target, as muscle twitches induced by stimulation could introduce confounding effects. Our study used sham as a control, thereby minimizing confounding factors like muscle twitches and enhancing comparability.

Interestingly, no significant HBC effects were observed at the 5cm target (Fig. 3b, Table1), which contrasts with findings from a recent study reporting strong individual responses at this target for six out of ten participants (Eva Dijkstra et al., 2023; E. Dijkstra et al., 2023). This discrepancy likely reflects individual variability, highlighting the complexity of HBC modulation.

4.2 Stimulation Intensity: Sub- and Supra-Threshold Stimulation

Stimulation intensity is a critical parameter influencing the effect of TMS (Hartwigsen & Silvanto, 2023; Numssen et al., 2024). While subthreshold rTMS has been shown to induce structural synaptic plasticity in animal models (Tang et al., 2021) and modulate cognitive processes in humans (Kuhnke et al., 2017), its influence on heart rate or other heart-brain axis-related states remains inconclusive (Crewther et al., 2022). In contrast, suprathreshold or threshold-level stimulation, which induces action potentials, has been found to regulate heart-brain coupling (Iseger et al., 2017; Iseger et al., 2021).

Nevertheless, our results indicate that HBC modulation is not solely dependent on stimulation intensity but also critically influenced by the target site, revealing a more complex, nonlinear interaction between these factors. As shown in Fig. 3a, the relationship between stimulation intensity (%MT) and HBC varies significantly across different DLPFC stimulation sites. Notably, at certain stimulation sites (e.g., F3 lateral, F3 posterior and F3 medial), HBC increases significantly at approximately suprathreshold or threshold-level stimulation, whereas other sites (e.g., F3) require lower stimulation intensities to produce modulate effects. This finding challenges the conventional assumption that a single MT is sufficient to define effective stimulation parameters for all cortical targets. Instead, it suggests that the functional threshold for DLPFC rTMS may differ from the standard MT, underscoring the need for HBC-based markers to guide individualized rTMS dosing (Numssen et al., 2024). Further research is needed to

assess if this metric to determine DLPFC stimulation thresholds can be used to effectively individualize DLPFC rTMS dosing.

4.3 Repeatability

For most targets, the repeatability of HBC induced by DLPFC NCG-TMS 2.0 was found to be relatively low across three repeated sessions, even for some that exhibited a significant intensity effect on HBC (F3, F3 medial, and F3 posterior). Only F3 anterior and F3 lateral (for higher stimulation intensity) showed moderate repeatability (Fig. 4, left panels).

Interestingly, we observed greater repeatability between Sessions 2 and 3, compared to between either of these and Session 1, particularly in the F3 anterior and F3 lateral (Fig. 4, right panels). This may reflect pre-intervention activities during Session 0, which could have induced fatigue or stress—factors known to significantly influence heart rate (Matuz et al., 2021; Thayer et al., 2012) during Session 1– or novelty effects of TMS. By Sessions 2 and 3, participants were likely more comfortable with the procedures, reducing procedural novelty effects seen in Session 1. Similar effects have been noted in studies where patients showed initial heart rate deceleration that was not observed in follow-up assessments after 30 days of rTMS treatments (Alario et al., 2024). These findings highlight the importance of considering session-specific factors and adaptation effects when interpreting heart rate dynamics.

4.4 Heart Rate Modulation by Pain and other Side Effects

Besides cortical stimulation by TMS, also nerves and muscle beneath the scalp can be activated by TMS in a site-specific manner, potentially inducing pain and pain-related perceptions and emotions, such as fear. As pain is known to affect heart rate, pain and other side effects were monitored during the experiments, quantified via questionnaires, and added to our statistical analyses to distinguish TMS-related from pain-related effects on heart rate. While pain and side effects influenced HBC to some extent, pain did non-linearly interact with the stimulation intensity on HBC, while other side effects generally increased HBC irrespective of other factors. Importantly, however, our analyses revealed that the intensity effect was not redundant with pain or other side effects.

Some degree of pain, a common side effect of TMS, can arise from directly activating nerves and muscles beneath the scalp. This nociceptive stimulation engages the autonomic nervous system, particularly the sympathetic branch, leading to fluctuations in heart rate (Porges, 1995). Additionally, pain can influence parasympathetic activity via v agus nerve engagement, further modulating the heart rate. Other side effects, such as facial muscle twitches (Proske & Gandevia, 2012), sensory alterations (Yang et al., 2024), and fatigue (Matuz et al., 2021) may influence both the sympathetic and parasympathetic nervous systems, thereby contributing to heart rate changes and alterations in HBC. Furthermore, TMS-induced emotional responses, such as fear, can increase sympathetic activity and elevate the heart rate (Messina et al., 2024). Paradoxically, fear may also trigger psychological stress that induces transient bradycardia via vagal activation (Forte et al., 2022). These bidirectional effects underscore the intricate relationship between autonomic regulation and TMS-induced side effects, which may explain the non-linear impact of TMS on HBC.

5. Conclusion

This study builds upon earlier discoveries by revealing that the NCG-TMS 2.0 protocol can profoundly influence heart activity (E. Dijkstra et al., 2023). Advancing beyond prior research, we uncover a systematic dependency on target location within the left DLPFC, alongside a non-linear HBC effect. Our findings indicate that HBC modulation varies with stimulation intensity across different DLPFC targets, with stimulation at F3 and nearby areas significantly enhancing HBC compared to sham stimulation. Furthermore, we unravel the effects of pain and other side effects on HBC, which, however, do not account for the modulation introduced by DLPFC stimulation. Although the repeatability within subjects is limited in the initial session, subsequent sessions yield more consistent results. Future investigations should explore the separation of TMS-induced electric fields from neural pathways, especially sgACC-DLPFC connectivity, to elucidate their influence on the autonomic system. These insights could deepen our understanding of the heart-brain axis and inform targeted therapeutic strategies.

6. Data availability

The full dataset is made available at https://osf.io/8qpv3/. All computational steps and related code are available at https://gitlab.gwdg.de/tms-localization/papers/tms-hbc.

7. Acknowledgments

We would like to express our sincere gratitude to Ariana Novak, Benjamin Kalloch, Jeremy Ranke, and Nico Leng for their invaluable contributions to the data collection process. We are also deeply thankful to Philipp Kuhnke for his insightful guidance and advice during the data analysis phase. Their efforts and expertise were integral to the success of this study.

8. Funding

This work was supported by Lise Meitner Excellence funding from the Max Planck Society, the European Research Council (ERC-2021-COG 101043747), and the German Research Foundation (HA 6314/3-1, HA 6314/4-2, HA 6314/9-1). Zijian was supported by the Deqing Hospital of Hangzhou Normal University. Ying Jing was supported by the China Scholarship Council. Ole Numssen and Konstantin Weise were supported by the Federal Ministry of Education Germany (Bundesministerium für Bildung und Forschung, BMBF, Grant no. 01GQ2201 to Thomas Knösche).

9. Conflict of interest

The authors declare that they have no known competing financial interests or personal relationships that

could have appeared to influence the work reported in this paper.

References

Alario, A. A., Pace, B. D., Niciu, M. J., & Trapp, N. T. (2023, Jun 23). Transcranial magnetic stimulation induces heart rate decelerations independent of treatment outcome. *Brain Stimul, 16*(4), 1044-1046. https://doi.org/10.1016/j.brs.2023.06.005

Alario, A. A., Pace, B. D., Niciu, M. J., & Trapp, N. T. (2024, Sep 26). Transcranial magnetic stimulation-associated heart rate decelerations attenuate after a TMS treatment course for depression. *Brain Stimul, 17*(5), 1155-1156. https://doi.org/10.1016/j.brs.2024.09.011

Bates, D., Mächler, M., Bolker, B., & Walker, S. (2015, 10/07). Fitting Linear Mixed-Effects Models Using lme4. *Journal of Statistical Software, 67*(1), 1 - 48. https://doi.org/10.18637/jss.v067.i01

Berger, S., Kliem, A., Yeragani, V., & Bar, K. J. (2012, Jul). Cardio-respiratory coupling in untreated patients with major depression. *J Affect Disord, 139*(2), 166-171. https://doi.org/10.1016/j.jad.2012.01.035

Cheng, C., Jiao, Y., Jia, M., Jin, J., Peng, X., Zhang, M., Song, X., Chu, Z., Zeng, X., Sun, J. B., Yang, X. J., & Qin, W. (2024, Sep 16). Neuro-cardiac coupling predicts heart rate regulation effects of neuro-cardiac-guided transcranial magnetic stimulation (TMS). *Brain Stimul, 17*(5), 1134-1136. https://doi.org/10.1016/j.brs.2024.09.007

Cole, E. J., Phillips, A. L., Bentzley, B. S., Stimpson, K. H., Nejad, R., Barmak, F., Veerapal, C., Khan, N., Cherian, K., Felber, E., Brown, R., Choi, E., King, S., Pankow, H., Bishop, J. H., Azeez, A., Coetzee, J., Rapier, R., Odenwald, N., Carreon, D., Hawkins, J., Chang, M., Keller, J., Raj, K., DeBattista, C., Jo, B., Espil, F. M., Schatzberg, A. F., Sudheimer, K. D., & Williams, N. R. (2022, Feb). Stanford Neuromodulation Therapy (SNT): A Double-Blind Randomized Controlled Trial. *Am J Psychiatry, 179*(2), 132-141. https://doi.org/10.1176/appi.ajp.2021.20101429

Crewther, B. T., Kasprzycka, W., Cook, C. J., & Rola, R. (2022, Jan). Impact of one HF-rTMS session over the DLPFC and motor cortex on acute hormone dynamics and emotional state in healthy adults: a sham-controlled pilot study. *Neurol Sci, 43*(1), 651-659. https://doi.org/10.1007/s10072-021-05335-7

Delignette-Muller, M. L., & Dutang, C. (2015, 03/20). fitdistrplus: An R Package for Fitting Distributions. *Journal of Statistical Software, 64*(4), 1 - 34. https://doi.org/10.18637/jss.v064.i04

Dijkstra, E., van Dijk, H., Vila-Rodriguez, F., Zwienenberg, L., Rouwhorst, R., Coetzee, J. P., Blumberger, D. M., Downar, J., Williams, N., Sack, A. T., & Arns, M. (2023, Oct). Transcranial Magnetic Stimulation-Induced Heart-Brain Coupling: Implications for Site Selection and Frontal Thresholding-Preliminary Findings. *Biol Psychiatry Glob Open Sci, 3*(4), 939-947. https://doi.org/10.1016/j.bpsgos.2023.01.003

Dijkstra, E. S. A., Frandsen, S. B., van Dijk, H., Duecker, F., Taylor, J. J., Sack, A. T., Arns, M., & Siddiqi, S. H. (2024, 2024/07/01). Probing prefrontal-sgACC connectivity using TMS-induced heart–brain coupling. *Nature Mental Health, 2*(7), 809-817. https://doi.org/10.1038/s44220-024-00248-8

Feng, Z. J., Deng, X. P., Zhao, N., Jin, J., Yue, J., Hu, Y. S., Jing, Y., Wang, H. X., Knosche, T. R., Zang, Y. F., & Wang, J. (2022, Jun 16). Resting-State fMRI Functional Connectivity Strength Predicts Local Activity Change in the Dorsal Cingulate Cortex: A Multi-Target Focused rTMS Study. *Cereb Cortex, 32*(13), 2773-2784. https://doi.org/10.1093/cercor/bhab380

Forte, G., Troisi, G., Pazzaglia, M., Pascalis, V., & Casagrande, M. (2022, Jan 24). Heart Rate Variability and Pain: A Systematic Review. *Brain Sci, 12*(2). https://doi.org/10.3390/brainsci12020153

Fox, M. D., Buckner, R. L., White, M. P., Greicius, M. D., & Pascual-Leone, A. (2012, Oct 1). Efficacy of transcranial magnetic stimulation targets for depression is related to intrinsic functional connectivity with the subgenual cingulate. *Biol Psychiatry, 72*(7), 595-603. https://doi.org/10.1016/j.biopsych.2012.04.028

Giustiniani, A., Vallesi, A., Oliveri, M., Tarantino, V., Ambrosini, E., Bortoletto, M., Masina, F., Busan, P., Siebner, H. R., Fadiga, L., Koch, G., Leocani, L., Lefaucheur, J. P., Rotenberg, A., Zangen, A.,

Violante, I. R., Moliadze, V., Gamboa, O. L., Ugawa, Y., Pascual-Leone, A., Ziemann, U., Miniussi, C., & Burgio, F. (2022, Sep). A questionnaire to collect unintended effects of transcranial magnetic stimulation: A consensus based approach. *Clin Neurophysiol, 141*, 101-108. https://doi.org/10.1016/j.clinph.2022.06.008

Gramfort, A., Luessi, M., Larson, E., Engemann, D. A., Strohmeier, D., Brodbeck, C., Goj, R., Jas, M., Brooks, T., Parkkonen, L., & Hamalainen, M. (2013, Dec 26). MEG and EEG data analysis with MNE-Python. *Front Neurosci, 7*, 267. https://doi.org/10.3389/fnins.2013.00267

Grosshagauer, S., Woletz, M., Vasileiadi, M., Linhardt, D., Nohava, L., Schuler, A. L., Windischberger, C., Williams, N., & Tik, M. (2024, Sep). Chronometric TMS-fMRI of personalized left dorsolateral prefrontal target reveals state-dependency of subgenual anterior cingulate cortex effects. *Mol Psychiatry, 29*(9), 2678-2688. https://doi.org/10.1038/s41380-024-02535-3

Hartwigsen, G., & Silvanto, J. (2023, Oct). Noninvasive Brain Stimulation: Multiple Effects on Cognition. *Neuroscientist, 29*(5), 639-653. https://doi.org/10.1177/10738584221113806

Iseger, T. A., Arns, M., Downar, J., Blumberger, D. M., Daskalakis, Z. J., & Vila-Rodriguez, F. (2020, Jan-Feb). Cardiovascular differences between sham and active iTBS related to treatment response in MDD. *Brain Stimul, 13*(1), 167-174. https://doi.org/10.1016/j.brs.2019.09.016

Iseger, T. A., Padberg, F., Kenemans, J. L., Gevirtz, R., & Arns, M. (2017, Sep-Oct). Neuro-Cardiac-Guided TMS (NCG-TMS): Probing DLPFC-sgACC-vagus nerve connectivity using heart rate - First results. *Brain Stimul, 10*(5), 1006-1008. https://doi.org/10.1016/j.brs.2017.05.002

Iseger, T. A., Padberg, F., Kenemans, J. L., van Dijk, H., & Arns, M. (2021, May). Neuro-Cardiac-Guided TMS (NCG TMS): A replication and extension study. *Biol Psychol, 162*, 108097. https://doi.org/10.1016/j.biopsycho.2021.108097

Iseger, T. A., van Bueren, N. E. R., Kenemans, J. L., Gevirtz, R., & Arns, M. (2020, Jan-Feb). A frontal-vagal network theory for Major Depressive Disorder: Implications for optimizing neuromodulation techniques. *Brain Stimul, 13*(1), 1-9. https://doi.org/10.1016/j.brs.2019.10.006

Jiao, Y., Cheng, C., Jia, M., Chu, Z., Song, X., Zhang, M., Xu, H., Zeng, X., Sun, J. B., Qin, W., & Yang, X. J. (2024, Oct). Neuro-cardiac-guided transcranial magnetic stimulation: Unveiling the modulatory effects of low-frequency and high-frequency stimulation on heart rate. *Psychophysiology, 61*(10), e14631. https://doi.org/10.1111/psyp.14631

Kaur, M., Michael, J. A., Hoy, K. E., Fitzgibbon, B. M., Ross, M. S., Iseger, T. A., Arns, M., Hudaib, A. R., & Fitzgerald, P. B. (2020, May-Jun). Investigating high- and low-frequency neuro-cardiac-guided TMS for probing the frontal vagal pathway. *Brain Stimul, 13*(3), 931-938. https://doi.org/10.1016/j.brs.2020.03.002

Koenig, J., Kemp, A. H., Beauchaine, T. P., Thayer, J. F., & Kaess, M. (2016, Jun). Depression and resting state heart rate variability in children and adolescents - A systematic review and meta-analysis. *Clin Psychol Rev, 46*, 136-150. https://doi.org/10.1016/j.cpr.2016.04.013

Kuhnke, P., Meyer, L., Friederici, A. D., & Hartwigsen, G. (2017, Mar 1). Left posterior inferior frontal gyrus is causally involved in reordering during sentence processing. *Neuroimage, 148*, 254-263. https://doi.org/10.1016/j.neuroimage.2017.01.013

Lefaucheur, J. P., Aleman, A., Baeken, C., Benninger, D. H., Brunelin, J., Di Lazzaro, V., Filipovic, S. R., Grefkes, C., Hasan, A., Hummel, F. C., Jaaskelainen, S. K., Langguth, B., Leocani, L., Londero, A., Nardone, R., Nguyen, J. P., Nyffeler, T., Oliveira-Maia, A. J., Oliviero, A., Padberg, F., Palm, U., Paulus, W., Poulet, E., Quartarone, A., Rachid, F., Rektorova, I., Rossi, S., Sahlsten, H., Schecklmann, M., Szekely, D., & Ziemann, U. (2020, Feb). Evidence-based guidelines on the therapeutic use of repetitive transcranial magnetic stimulation (rTMS): An update (2014-2018). *Clin Neurophysiol, 131*(2), 474-528. https://doi.org/10.1016/j.clinph.2019.11.002

Lüdecke, D. (2018). ggeffects: Tidy data frames of marginal effects from regression models. *Journal of Open*

Source Software, 3(26), 772. https://doi.org/10.21105/joss.00772

Lüdecke, D. (2024). *sjPlot: Data Visualization for Statistics in Social Science. R package version 2.8.17*. https://CRAN.R-project.org/package=sjPlot

Lüdecke, D., Ben-Shachar, M. S., Patil, I., Waggoner, P., & Makowski, D. (2021). performance: An R package for assessment, comparison and testing of statistical models. *Journal of Open Source Software, 6*(60). https://doi.org/10.21105/joss.03139

Makowski, D., Ben-Shachar, M. S., Patil, I., & Lüdecke, D. (2020). Methods and algorithms for correlation analysis in R. *Journal of Open Source Software, 5*(51), 2306. https://doi.org/10.21105/joss.02306

Makowski, D., Pham, T., Lau, Z. J., Brammer, J. C., Lespinasse, F., Pham, H., Scholzel, C., & Chen, S. H. A. (2021, Aug). NeuroKit2: A Python toolbox for neurophysiological signal processing. *Behav Res Methods, 53*(4), 1689-1696. https://doi.org/10.3758/s13428-020-01516-y

Martin, S., Frieling, R., Saur, D., & Hartwigsen, G. (2023, Sep-Oct). TMS over the pre-SMA enhances semantic cognition via remote network effects on task-based activity and connectivity. *Brain Stimul, 16*(5), 1346-1357. https://doi.org/10.1016/j.brs.2023.09.009

Matuz, A., van der Linden, D., Kisander, Z., Hernadi, I., Kazmer, K., & Csatho, A. (2021). Enhanced cardiac vagal tone in mental fatigue: Analysis of heart rate variability in Time-on-Task, recovery, and reactivity. *PLoS One, 16*(3), e0238670. https://doi.org/10.1371/journal.pone.0238670

Messina, G., Monda, A., Messina, A., Di Maio, G., Monda, V., Limone, P., Dipace, A., Monda, M., Polito, R., & Moscatelli, F. (2024, Apr 28). Relationship between Non-Invasive Brain Stimulation and Autonomic Nervous System. *Biomedicines, 12*(5). https://doi.org/10.3390/biomedicines12050972

Mir-Moghtadaei, A., Caballero, R., Fried, P., Fox, M. D., Lee, K., Giacobbe, P., Daskalakis, Z. J., Blumberger, D. M., & Downar, J. (2015, Sep-Oct). Concordance Between BeamF3 and MRI-neuronavigated Target Sites for Repetitive Transcranial Magnetic Stimulation of the Left Dorsolateral Prefrontal Cortex. *Brain Stimul, 8*(5), 965-973. https://doi.org/10.1016/j.brs.2015.05.008

Niehaus, L., Guldin, B., & Meyer, B. (2001, Jan 1). Influence of transcranial magnetic stimulation on pupil size. *J Neurol Sci, 182*(2), 123-128. https://doi.org/10.1016/s0022-510x(00)00462-7

Numssen, O., Kuhnke, P., Weise, K., & Hartwigsen, G. (2024). Electric-field-based dosing for TMS. *Imaging Neuroscience, 2*, 1-12. https://doi.org/10.1162/imag_a_00106

Numssen, O., van der Burght, C. L., & Hartwigsen, G. (2023, Jun). Revisiting the focality of non-invasive brain stimulation - Implications for studies of human cognition. *Neurosci Biobehav Rev, 149*, 105154. https://doi.org/10.1016/j.neubiorev.2023.105154

Oldfield, R. C. (1971, Mar). The assessment and analysis of handedness: the Edinburgh inventory. *Neuropsychologia, 9*(1), 97-113. https://doi.org/10.1016/0028-3932(71)90067-4

Pascual-Leone, A., Rubio, B., Pallardo, F., & Catala, M. D. (1996, Jul 27). Rapid-rate transcranial magnetic stimulation of left dorsolateral prefrontal cortex in drug-resistant depression. *Lancet, 348*(9022), 233-237. https://doi.org/10.1016/s0140-6736(96)01219-6

Polomano, R. C., Galloway, K. T., Kent, M. L., Brandon-Edwards, H., Kwon, K. N., Morales, C., & Buckenmaier, C., 3rd. (2016, Aug). Psychometric Testing of the Defense and Veterans Pain Rating Scale (DVPRS): A New Pain Scale for Military Population. *Pain Med, 17*(8), 1505-1519. https://doi.org/10.1093/pm/pnw105

Porges, S. W. (1995, Summer). Cardiac vagal tone: a physiological index of stress. *Neurosci Biobehav Rev, 19*(2), 225-233. https://doi.org/10.1016/0149-7634(94)00066-a

Proske, U., & Gandevia, S. C. (2012, Oct). The proprioceptive senses: their roles in signaling body shape, body position and movement, and muscle force. *Physiol Rev, 92*(4), 1651-1697.

https://doi.org/10.1152/physrev.00048.2011

Rossi, S., Antal, A., Bestmann, S., Bikson, M., Brewer, C., Brockmoller, J., Carpenter, L. L., Cincotta, M., Chen, R., Daskalakis, J. D., Di Lazzaro, V., Fox, M. D., George, M. S., Gilbert, D., Kimiskidis, V. K., Koch, G., Ilmoniemi, R. J., Lefaucheur, J. P., Leocani, L., Lisanby, S. H., Miniussi, C., Padberg, F., Pascual-Leone, A., Paulus, W., Peterchev, A. V., Quartarone, A., Rotenberg, A., Rothwell, J., Rossini, P. M., Santarnecchi, E., Shafi, M. M., Siebner, H. R., Ugawa, Y., Wassermann, E. M., Zangen, A., Ziemann, U., Hallett, M., & basis of this article began with a Consensus Statement from the Ifcn Workshop on "Present, F. o. T. M. S. S. E. G. S. O. u. t. A. (2021, Jan). Safety and recommendations for TMS use in healthy subjects and patient populations, with updates on training, ethical and regulatory issues: Expert Guidelines. *Clin Neurophysiol*, *132*(1), 269-306. https://doi.org/10.1016/j.clinph.2020.10.003

Rossini, P. M., Burke, D., Chen, R., Cohen, L. G., Daskalakis, Z., Di Iorio, R., Di Lazzaro, V., Ferreri, F., Fitzgerald, P. B., George, M. S., Hallett, M., Lefaucheur, J. P., Langguth, B., Matsumoto, H., Miniussi, C., Nitsche, M. A., Pascual-Leone, A., Paulus, W., Rossi, S., Rothwell, J. C., Siebner, H. R., Ugawa, Y., Walsh, V., & Ziemann, U. (2015, Jun). Non-invasive electrical and magnetic stimulation of the brain, spinal cord, roots and peripheral nerves: Basic principles and procedures for routine clinical and research application. An updated report from an I.F.C.N. Committee. *Clin Neurophysiol*, *126*(6), 1071-1107. https://doi.org/10.1016/j.clinph.2015.02.001

Rouwhorst, R., van Oostrom, I., Dijkstra, E., Zwienenberg, L., van Dijk, H., & Arns, M. (2022, Sep-Oct). Vasovagal syncope as a specific side effect of DLPFC-rTMS: A frontal-vagal dose-finding study. *Brain Stimul*, *15*(5), 1233-1235. https://doi.org/10.1016/j.brs.2022.08.015

Schmausser, M., Raab, M., & Laborde, S. (2024, Sep). The dynamic role of the left dlPFC in neurovisceral integration: Differential effects of theta burst stimulation on vagally mediated heart rate variability and cognitive-affective processing. *Psychophysiology*, *61*(9), e14606. https://doi.org/10.1111/psyp.14606

Spellman, T., & Liston, C. (2020, May 1). Toward Circuit Mechanisms of Pathophysiology in Depression. *Am J Psychiatry*, *177*(5), 381-390. https://doi.org/10.1176/appi.ajp.2020.20030280

Tang, A. D., Bennett, W., Bindoff, A. D., Bolland, S., Collins, J., Langley, R. C., Garry, M. I., Summers, J. J., Hinder, M. R., Rodger, J., & Canty, A. J. (2021, Nov-Dec). Subthreshold repetitive transcranial magnetic stimulation drives structural synaptic plasticity in the young and aged motor cortex. *Brain Stimul*, *14*(6), 1498-1507. https://doi.org/10.1016/j.brs.2021.10.001

Thayer, J. F., Ahs, F., Fredrikson, M., Sollers, J. J., 3rd, & Wager, T. D. (2012, Feb). A meta-analysis of heart rate variability and neuroimaging studies: implications for heart rate variability as a marker of stress and health. *Neurosci Biobehav Rev*, *36*(2), 747-756. https://doi.org/10.1016/j.neubiorev.2011.11.009

Thayer, J. F., & Lane, R. D. (2009, Feb). Claude Bernard and the heart-brain connection: further elaboration of a model of neurovisceral integration. *Neurosci Biobehav Rev*, *33*(2), 81-88. https://doi.org/10.1016/j.neubiorev.2008.08.004

Thut, G., Veniero, D., Romei, V., Miniussi, C., Schyns, P., & Gross, J. (2011, Jul 26). Rhythmic TMS causes local entrainment of natural oscillatory signatures. *Curr Biol*, *21*(14), 1176-1185. https://doi.org/10.1016/j.cub.2011.05.049

Vallat, R. (2018). Pingouin: statistics in Python. *Journal of Open Source Software*, *3*(31), 1026. https://doi.org/10.21105/joss.01026

Verberne, A. J., & Owens, N. C. (1998, Feb). Cortical modulation of the cardiovascular system. *Prog Neurobiol*, *54*(2), 149-168. https://doi.org/10.1016/s0301-0082(97)00056-7

Virtanen, P., Gommers, R., Oliphant, T. E., Haberland, M., Reddy, T., Cournapeau, D., Burovski, E., Peterson, P., Weckesser, W., Bright, J., van der Walt, S. J., Brett, M., Wilson, J., Millman, K. J., Mayorov, N., Nelson, A. R. J., Jones, E., Kern, R., Larson, E., Carey, C. J., Polat, I., Feng, Y., Moore, E. W., VanderPlas, J., Laxalde, D., Perktold, J., Cimrman, R., Henriksen, I., Quintero, E. A., Harris, C. R., Archibald, A. M., Ribeiro, A. H., Pedregosa, F., van Mulbregt, P., & SciPy, C. (2020, Mar). SciPy 1.0: fundamental algorithms for scientific computing in Python. *Nat Methods*, *17*(3), 261-272.

https://doi.org/10.1038/s41592-019-0686-2

Wood, S. N. (2017). *Generalized additive models: an introduction with R*. chapman and hall/CRC.

Yang, W., Chen, T., He, R., Goossens, R., & Huysmans, T. (2024, Jan). Autonomic responses to pressure sensitivity of head, face and neck: Heart rate and skin conductance. *Appl Ergon*, *114*, 104126. https://doi.org/10.1016/j.apergo.2023.104126

Zwienenberg, L., Iseger, T. A., Dijkstra, E., Rouwhorst, R., van Dijk, H., Sack, A. T., & Arns, M. (2021, Sep-Oct). Neuro-cardiac guided rTMS as a stratifying method between the '5cm' and 'BeamF3' stimulation clusters. *Brain Stimul*, *14*(5), 1070-1072. https://doi.org/10.1016/j.brs.2021.07.005